Green Synthesis and Morphology of Nano Yttria Mediated by *Agaricus bisporus*

K.B. Satishkumar[1], T.K. Vishnuvardhan[2,*], B. Rajashekhar[3], K. Satish[1], Shashidhar[3] and B. Sreekanth[4]

[1]Department of Chemistry, Acharya Institute of Technology, Achith Nagar Post, Soladevanahalli, Bengaluru-560107, India
[2]Department of Chemistry, Ramaiah University of Applied Sciences, Peenya Campus, Bengaluru-560058, India
[3]Department of Chemistry, SDM College of Engineering and Technology, Dharwad-580002, India
[4]Department of Chemical Engineering, SDM College of Engineering and Technology, Dharwad-580002, India

*Corresponding author: E-mail: vishnu33vardhan@gmail.com

Nano-yttrium oxide has been synthesized from yttrium nitrate hexahydrate by combustion of *Agarics bisporus* (mushroom) used as fuel. The precursor yttirium nitrate and fuel in acid medium are combusted in furnace at 400 ºC for 3 h yields yttria nanopowder. Morphology of the reaction products are characterized by SEM and TEM. Synthesized yttria nanoparticle are characterized by UV, FTIR, XRD and EDAX are discussed. The crystallite size obtained nano yttria particles are calculated by Scherer's equation and compared with Williamson-Hall method.

Keywords: *Agarics bisporus*, Yttrium oxide, Green synthesis, Solid state combustion.

INTRODUCTION

Rare earth element like nano-Y_2O_3 is used as a antioxidant for nerve cell HT22. In the absence of the nanoparticles nerve cells stimulate the enhanced reactive oxygen species due to oxidative stress and cause the oxidative damage in animal. Such a oxidative stress and oxidative damage in animals can be regulated by cerium or yttrium nanoparticles [1]. High dielectric strength of the yttria proposed to replace SiO_2 films in electronic devices. Yttria powders can be used as a precursor for the synthesis of dense ceramic objects. Synthesis of yttria by photosynthesis oxidation of yttrium nanoparticles are used during the removal of byproducts [2]. Yttria nanoparticles synthesis by co-precipitation method gives unique structural properties to use in optical studies [3].

Yttrium oxide has been synthesized by a combustion synthesis process using various fuels [4,5]. It has been noted that the choice of fuel alters exothermicity of combustion reaction, which has a strong influence on the properties of the product [5]. Microstructure evolution by increasing the calcination temperature of nano-yttrium oxide synthesized by combustion using ethylene glycol as a fuel [6].

Green synthesis for nanoparticles has a great interest of study, due to the distinct properties of nanoparticles and their applications. Synthesis of yttrium-aluminium garnet by co-precipitation and effect of precipitant has described the morphological change impact on the dispersibility and excellent sinterability [7]. Yttrium oxide with cubic symmetry is one of the important oxide host for the solid state laser, as well as far infrared ceramics [8]. Eu doped Y_2O_3 is a well known red phosphorous and it has been proposed that replacement for SiO_2 for dielectric films in electronic devices because of high dielectric strength and low leak current [2]. Y_2O_3 nanoparticles are synthesized by low cost modified transient morphology method. This method is attracted much attention because of convenient process and needing simple instrument. The transient morphology method is based on combustion synthesis and introduced by Mouzon *et al.* [9] for Y_2O_3 nanoparticles synthesis. Europium doped nano-yttria synthesized by sucrose templated combustion method showed applications in red emitting phosphorous used in CRT screens, plasma display systems and fluorescent lamps [11].

The fresh edible button mushroom (*Agaricus bisporus*) commercial available were utilized for cooking as nutritious

food having 93 KJ of energy and also possess medical applications especially to treat breast cancer. Button mushroom constitutes the nutritive compounds of water/moisture, soluble carbohydrates and proteins, vitamins, minerals, electrolytes (P, K, Mg) and trace elements (Fe, Na, Zn). There is a report of biological synthesis of silver nanoparticles by using button mushroom [12].

In present work, we report the preparation of Y_2O_3 nanoparticles and their characterization by UV, IR, XRD and morphology of yttria nanoparticles are studied with SEM and TEM. Yttria nanoparticles are anticipated to use in ammonia, methane, LPG gas sensor studies.

EXPERIMENTAL

Muffle furnace Model RK Enterprises, Chennai (India) 800 g capacity. UV-visible measurements were recorded using an SL159 ELICO. UV-Visible spectrometer in the wavelength range 200-600 nm by dispersing the compound in alcoholic media. Fourier transform infrared spectroscopy (FT-IR) was performed by using a Perkin-Elmer spectrometer (Spectrum 1000) using KBr pellets. The powder X-ray diffraction (PXRD) patterns were recorded using Shimadzu (MAXima_XRD-7000) made with CuK_α radiation in the range of 10-80° and λ = 1.54. Morphology of the samples and particles size were examined by scanning electronmicroscope (SEM, Hitachi-3000) and transmission electron microscope (TEM, TECNAIF-30).

Precursor yttrium nitrate hexahydrate is mixed in the minimum amount of water and nitric acid and stirred thoroughly to obtain homogeneous solution in a silica crucible. Fuel *Agaricus bisporus* or button shape mushroom is dried and powdered by using mechanical grinding. Finally grounded *Agaricus bisporus* is mixed with yttrium nitrate solution in silica crucible. The mixture is heated over muffle furnace at 375-400 K. When the temperature of the solution goes beyond 373 K solution begin to boil and forming foam with liberation of oxides of carbon, sulphur and nitrogen of the mushroom resulting in the reddish brown fumes followed by foamy yellowish mass.

Once the fumes ceases then the foamy yellowish mass is placed in furnace and heated to 500 °C for 3-4 h then cool to room temperature normally. Weight percentages of the yttria and fuel varied by (a) 0.5-0.5, (b) 1.0-0.5 and (c) 1.0-1.5 yielded 1.460, 1.4267 and 1.1077 g, respectively. Similarly, nano-yttria plan to prepare in alkali media but failed to get the expected product.

RESULTS AND DISCUSSION

UV analysis: Powdered nano-yttria are shown in Fig. 1 prepared in 0.5-0.5 proportion of precursor and fuel samples. It clearly indicates that the λ_{max} for yttria in 0.5 -0.5 precursor to fuel combination has 225 nm and that of 1.0-1.5 has 221 nm. The direct forbidden energy gap obtained by extrapolating the line for λ_{max} curve which intersect at x-axis and whose wavelength are 255 and 235 nm (Fig. 1), band gap calculated for a sample is 4.86 and for sample (b) is 5.27, the obtained band gap well matched with the literature value [13].

IR analysis: FTIR of samples a, b and c are shown in Fig. 2. The peaks at 621 and 721 cm^{-1} may be assigned to Y-O stretching originated from Y_2O_3, while the peak at 1731 cm^{-1} may be assigned to asymmetric stretching of C-O of CO_2, small amount of CO_2 may be due to presence of fuel or atmospheric carbon dioxide, which may arise due to the absorption of CO_2 from the atmosphere. Another notable peak at 3561 cm^{-1} may be due to the presence of O-H of water molecule. The lower wave number side of the as-prepared samples. It is understood that the decrease in the particle size enhances the surface effects which in turn enlarge the absorption. Thus, the Y-O absorption bands are widened [14,15].

XRD analysis: XRD patterns of the samples with different proportions of precursor and fuel showed multiphase evolution from the distorted structure to cubic Y_2O_3 phase. Pattern of a dried as-prepared product had three very weak and broad peaks at about 30°-28°, 42° and 56°. The XRD patterns of the samples annealed at 500 °C resembled that of the as-prepared literature [16], but the peak at around 28° gradually shifted toward
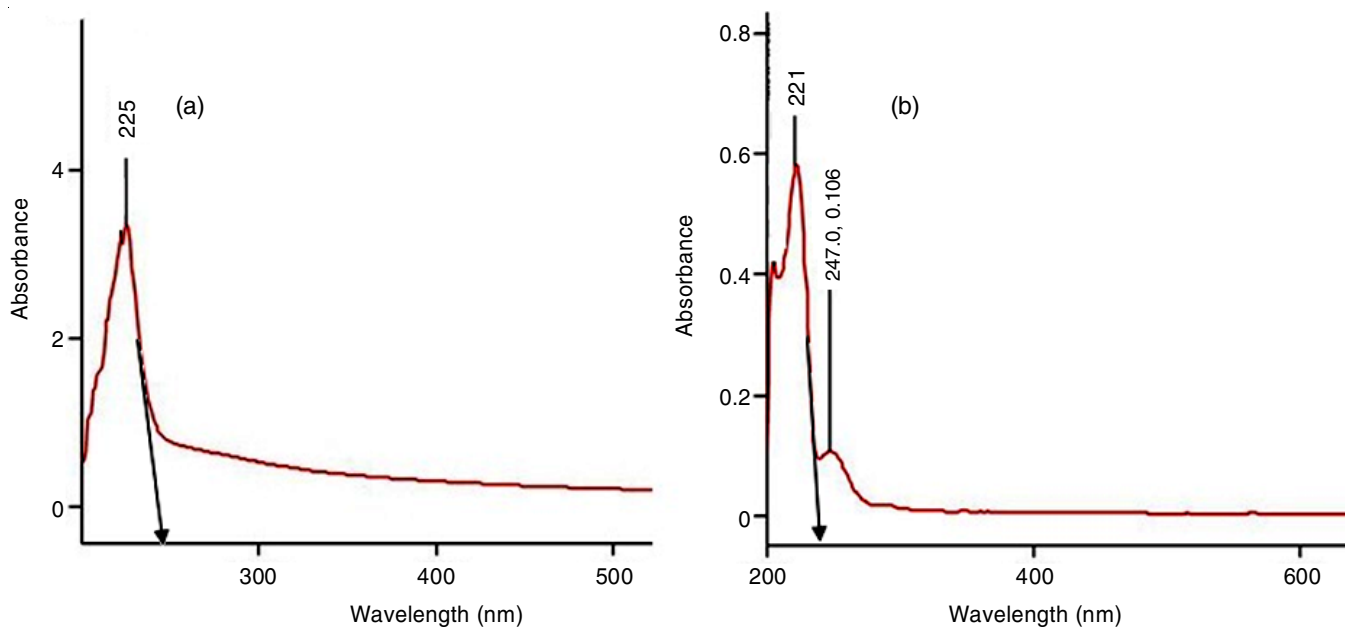

Fig. 1. UV spectra of nano-yttria obtained in two ratios a) 0.5-0.5 and b) 1.0-1.5 of precursor and fuel
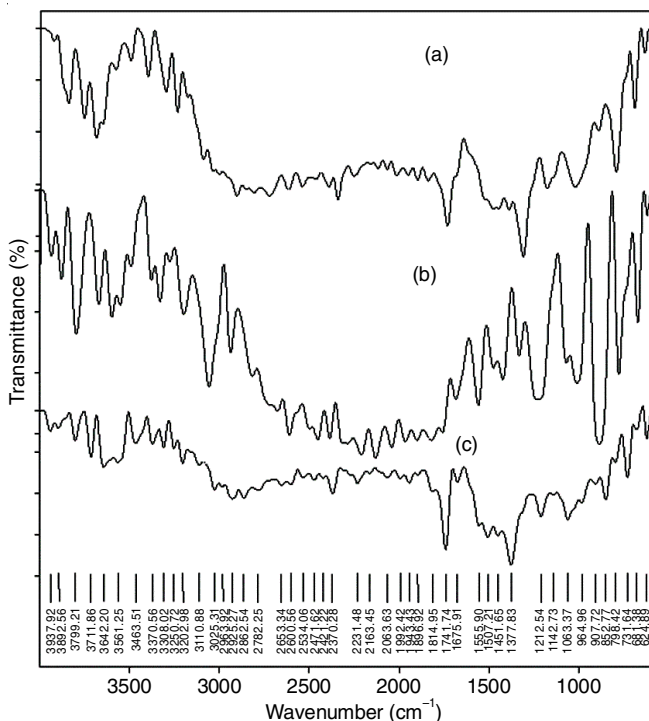
Fig. 2. FTIR spectra of nano-yttria obtained in three different ratios a) 0.5-0.5, b) 1.0-0.5 and c) 1.0-1.5 of precursor and fuel

a higher angle closer to the strongest peak of cubic Y_2O_3 phase at 30° (222). This peak finally became the strongest cubic Y_2O_3 phase at ~30. (Fig. 3). Therefore, the structure of as-prepared yttrium oxide nanoparticle was related to the cubic Y_2O_3 phase. The other peaks of the planes are less intense.
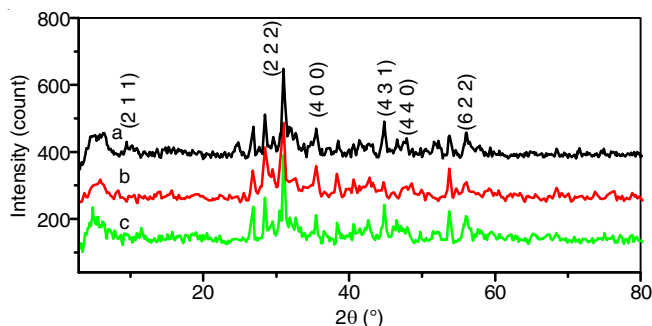

Fig. 3. XRD of the nano yttria obtained by using the precursor to fuel ratios are a) 0.5-0.5, b) 1.0-0.5 and c) 1.0-1.5

Some relatively narrow and stronger peaks at 30, 42 and 55 appeared. In fact, these peaks were found in the sample with all different ratios shows the cubic Y_2O_3 phase. The above synthesized yttria phases well matches with the recent literature and in the JCPDS 89-5592 database, these peaks are assigned as 1 3 4, 4 4 0 and 6 2 2. All above phase are also found in synthesized yttria with different ratios. The peaks became stronger and sharper, indicating larger and better-crystallized. Similar yttria also prepared from yttrium nitrate decomposition at different anneling temperature broadly discussed by X-ray analysis [16]. Further, XRD patterns are supported by bismuth and zinc, and co-doped with yttria studies for optical studies prepared by solvothermal and wet-chemical method [17].

The estimated ranges of particle sizes measured from TEM photographs and the average sizes of the crystalline regions calculated from XRD peak broadening of the annealed samples are listed in Table-1. Due to particle aggregation, the accuracy of particle size estimation fromTEM photographs is limited. The average sizes of crystalline regions in the annealed samples were calculated from XRD. Particles sizes are calculated using intense peaks from the XRD by using Scherrer's equation:

$$D = \frac{k\lambda}{\beta\cos\theta}$$

where, D is the particle size in nm, λ is the wavelength of radiation ($\lambda = 1.54$ Å), β is the full width at half maximum (FWHM) intensity, θ is the peak position and k is a constant equal to 0.9. Williamson-Hall method (W-H method) [18] was used to calculate particle size and strain induced broadening. In this method, graph was plotted with $\beta\cos\theta$ *versus* $4\sin\theta$ and the particle size was calculated which is in good agreement with the value calculated from Scherrer equation. Table-1 shows the particle size of nanocomposites as calculated from both the methods. Further, size-strain plot model for each of the synthesized meal oxide from W-H plot gives the strain induced broadening value in the order of 0.0031 to 0.0063. It is observed that the strain induced in metal oxide during varies proportion of fuel to precursor. In this study, it is also seen that as the crystallite size of particles increases and decreases, strain induced in fuel to precursor ratio increases.

TABLE-1
COMPARISON OF PARTICLES SIZES BY
W–H METHOD AND SCHERER'S FORMULA

Samples label	Particle size by W–H method nm	Lattice strain	Particles size by Scherer's formula (nm)
a	22.00	0.0063	21
b	43.07	0.0031	43
c	34.46	0.0039	29

SEM analysis: Fig. 4(a-c) shows the morphological changes undergone by powder analysis as crystallite size precursor and fuel in different ratio shows a flake, tiny needle and foamy morphology in a, b and c samples respectively. In case of sample c, foam texture becomes porous. Similar, morphology of prepared Y_2O_3 by hydrothermal microwave method with different calcination temperature also obtained by Abdulghani and Al-Ogedy [19].

EDAX analysis: Fig. 5 shows the presence of composition of synthesized yttria, as the product is washed thoroughly and heated at high temperature records the purity. Composition of yttria can be supported from the peaks of oxygen and yttrium from the EDAX spectrum.

TEM analysis: Fig. 6 shows the TEM morphology for sample a, as grains are compacted and one-to-one grain adhesion, sample b shows much larger particles and less network-like aggregation (Fig. 6). However in sample c, grains are looks to larges but weak force of attraction resulted in weak interaction grain size is also small but more crystalline.

Conclusion

Synthesis of nano-yttrium oxides is successfully acheived from yttrium nitrate hexahydrate by combustion of *Agarics*
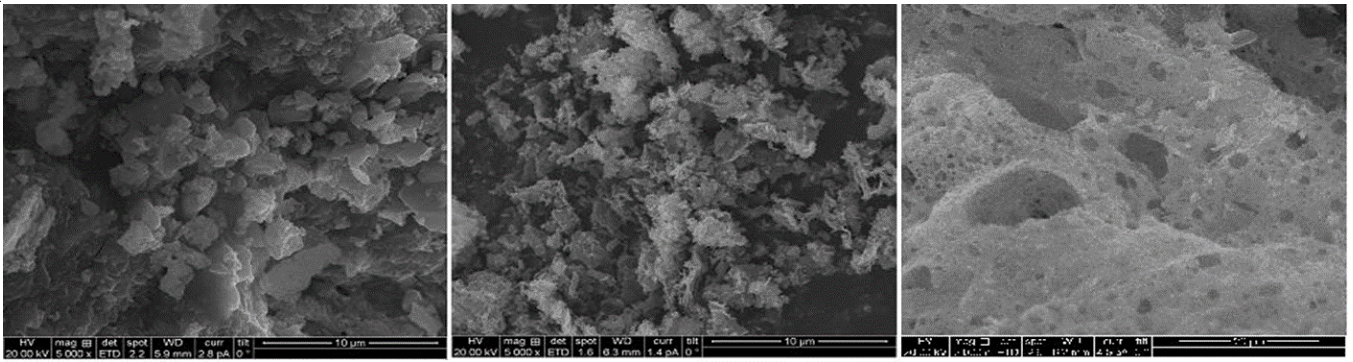
Fig. 4. SEM images of yttria nanopowder obtained in three different ratios a) 0.5-0.5, b) 1.0-0.5 and c) 1.0-1.5 of precursor and fuel
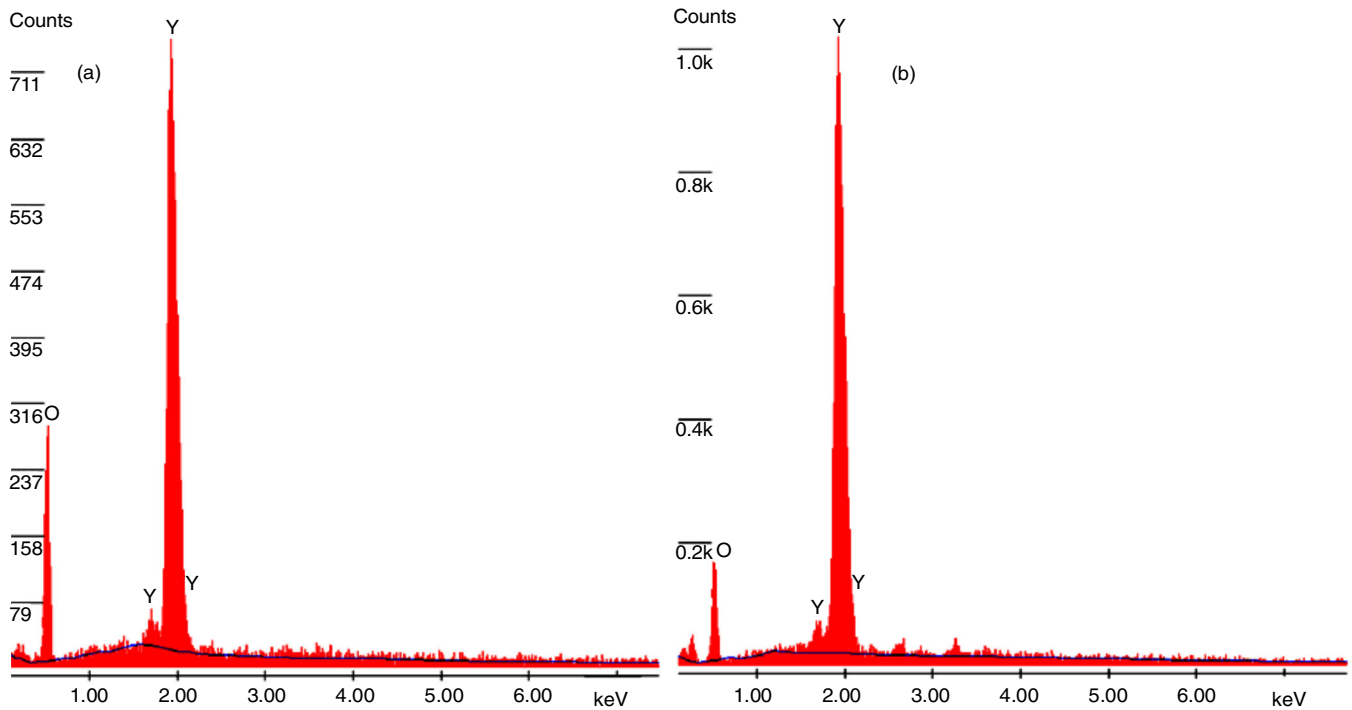

Fig. 5. EDAX spectra of yttria nanopowder obtained in two ratios a) 0.5-0.5 and b) 1.0-0.5 of precursor and fuel
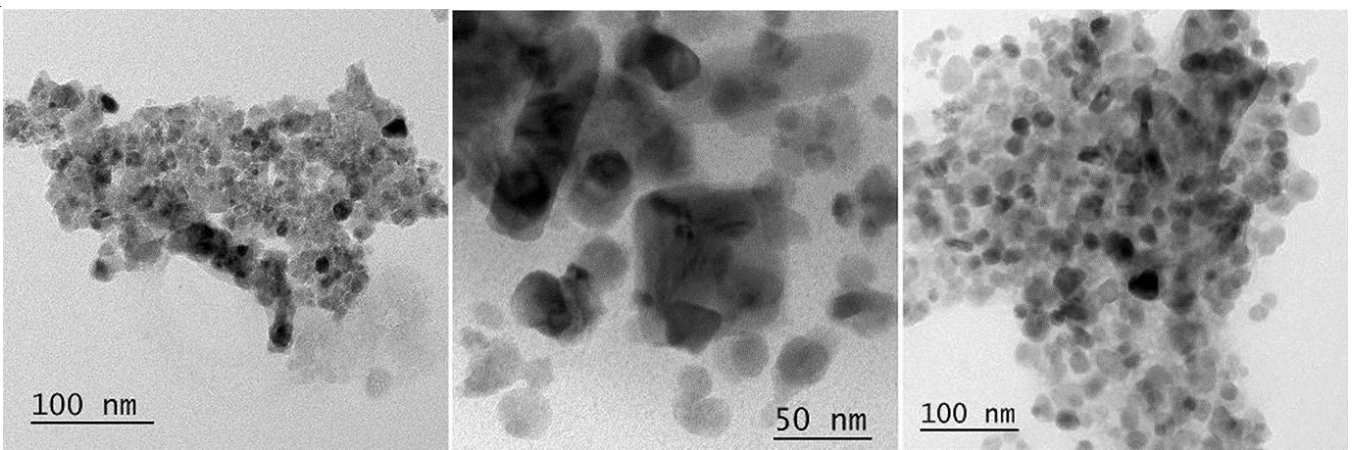

Fig. 6. TEM morphology of yttria nanopowder obtained in three different ratios a) 0.5-0.5, b) 1.0-0.5 and c) 1.0-1.5 of precursor and fuel

bisporus (mushroom) used as fuel. FTIR spectra indicates the presence of Y-O bonds, which can be further confirmed by EDAX analysis. The X-ray diffraction of synthesized nano-yttrium oxide indicates that structure is cubic having a particle sizes of 21, 43 and 29 nm, which is further confirmed from TEM analysis, which is found nearly same as 23, 46 and 27 nm. The SEM images shows the morphology of obtained nano-yttria samples as flakes, tiny needle and foamy.

CONFLICT OF INTEREST

The authors declare that there is no conflict of interests regarding the publication of this article.

REFERENCES

1. D. Schubert, R. Dargusch, J. Raitano and S.-W. Chan, *Biochem. Biophys. Res. Commun.*, **342**, 86 (2006);
   https://doi.org/10.1016/j.bbrc.2006.01.129.
2. J.A. Nelson and M.J. Wagner, *Chem. Mater.*, **14**, 915 (2002);
   https://doi.org/10.1021/cm010900u.
3. R. Srinivasan, R. Yogamalar and A.C. Bose, *Mater. Res. Bull.*, **45**, 1165 (2010);
   https://doi.org/10.1016/j.materresbull.2010.05.020.
4. S. Roy, W. Sigmund and F. Aldinger, *J. Mater. Sci. Lett.*, **16**, 1148 (1997);
   https://doi.org/10.1023/A:1018540506123.
5. S. Ekambaram and K.C. Patil, *J. Mater. Chem.*, **5**, 905 (1995);
   https://doi.org/10.1039/jm9950500905.
6. N. Dasgupta, R. Krishnamoorthy and K.T. Jacob, *Int. J. Inorg. Mater.*, **3**, 143 (2001);
   https://doi.org/10.1016/S1466-6049(00)00108-2.
7. J.-G. Li, T. Ikegami, J.-H. Lee, T. Mori and Y. Yajima, *J. Eur. Ceram. Soc.*, **20**, 2395 (2000);
   https://doi.org/10.1016/S0955-2219(00)00116-3.
8. R. Chaim, A. Shlayer and C. Estournes, *J. Eur. Ceram. Soc.*, **29**, 91 (2009);
   https://doi.org/10.1016/j.jeurceramsoc.2008.05.043.
9. J. Mouzon and M. Odén, *Powder Technol.*, **177**, 77 (2007);
   https://doi.org/10.1016/j.powtec.2007.02.045.
10. J. Dhanaraj, R. Jagannathan, T.R.N. Kutty and C.-H. Lu, *J. Phys. Chem. B*, **105**, 11098 (2001);
    https://doi.org/10.1021/jp0119330.
11. L. Xu, B. Wei, Z. Zhang, Z. Lü, H. Gao and Y. Zhang, *Nanotechnology*, **17**, 4327 (2006);
    https://doi.org/10.1088/0957-4484/17/17/008.
12. G. Narasimha, B. Praveen, K. Mallikarjuna and B.D. Prasad Raju, *Int. J. Nano Dimens.*, **2**, 29 (2011);
    https://doi.org/10.7508/IJND.2011.01.004.
13. S.G. Lim, S. Kriventsov, T.N. Jackson, J.H. Haeni, D.G. Schlom, A.M. Balbashov, R. Uecker, P. Reiche, J.L. Freeouf and G. Lucovsky, *J. Appl. Phys.*, **91**, 4500 (2002);
    https://doi.org/10.1063/1.1456246.
14. T. Mokkelbost, I. Kaus, T. Grande and M.A. Einarsrud, *Chem. Mater.*, **16**, 5489 (2004);
    https://doi.org/10.1021/cm048583p.
15. R. Srinivasan, R. Yogamalar and A.C. Bose, *Mater. Res. Bull.*, **45**, 1165 (2010);
    https://doi.org/10.1016/j.materresbull.2010.05.020.
16. R.P. Ermakov, V.V. Voronov and P.P. Fedorov, *Nanosystems: Phys. Chem. Math.*, **4**, 196 (2013).
17. G. Bhavani and S. Ganesan, *Acta Phys. Pol. A*, **130**, 1373 (2016);
    https://doi.org/10.12693/APhysPolA.130.1373.
18. S.T. Tan, B.J. Chen, X.W. Sun, W.J. Fan, H.S. Kwok, X.H. Zhang and S.J. Chua, *J. Appl. Phys.*, **98**, 013505 (2005);
    https://doi.org/10.1063/1.1940137.
19. J.A. Abdulghani and W.M. Al- Ogedy, *Iraqi J. Sci.*, **56C**, 1572 (2015).